

# Interaction of Energy Discharge and Hypersonic Vehicle

Nadia Kianvashrad\* and Doyle Knight\*†

\*Rutgers University

New Brunswick, NJ 08903, USA

nadiakianvashrad@gmail.com · doyleknight@gmail.com

†Corresponding author

## Abstract

The effect of off-axis energy deposition in front of a notional supersonic/hypersonic vehicle is studied as a means of flight control. The off-axis energy discharge creates a side force and changes the drag force and thus there is a change in the pitching moment. A parametric study is performed to examine the effect of energy added to the heated region (dimensionless energy parameter), the size of heated region relative to the body and freestream Mach number. The peak values of pitching moment coefficient due to energy deposition vary from 3.2% to 6.4% of the value corresponding to a 20° deflection of a finset; however, the time interval for the change in pitching moment coefficient due to the energy deposition is 44 to 88 times faster than the expected actuation time (0.1 s) for the finset, thus indicating the possibility for flight control using pulsed energy deposition.

## 1. Introduction

The interaction of an energy discharge (*e.g.*, laser, microwave, DC) with the shock system generated by a hypersonic vehicle causes momentary changes in the forces and moments acting on the vehicle.<sup>19,20</sup> Significant computational and experimental studies have demonstrated momentary drag reduction for energy discharge on-axis. Examples include Artemev *et al.*,<sup>3</sup> Tretyakov *et al.*,<sup>31</sup> Riggins *et al.*,<sup>27</sup> Wilkerson *et al.*,<sup>34</sup> Lashkov *et al.*,<sup>24</sup> Fomin *et al.*,<sup>11</sup> Adelgren *et al.*,<sup>1</sup> Kremeyer *et al.*,<sup>22</sup> Kuo,<sup>23</sup> Knight *et al.*,<sup>21</sup> Schülein *et al.*,<sup>29</sup> Kim *et al.*,<sup>17</sup> Erdem *et al.*,<sup>10</sup> Kianvashrad *et al.*,<sup>16</sup> Desai *et al.*,<sup>8</sup> Kianvashrad *et al.*<sup>15</sup> and Kianvashrad and Knight.<sup>14</sup> Knight<sup>20</sup> summarizes the state-of-the-art of energy deposition for flow control.

A more recent application of energy discharge is flight control. Pulsed energy discharge has the potential for rapid maneuvering of supersonic and hypersonic vehicles. In this regard, rapid maneuvering is defined as the ability to substantially change the forces and moments on a vehicle within the time required for the vehicle to travel a distance equal to its length. Conventional methods for flight control utilize deflected surfaces (*e.g.*, ailerons, fins) requiring on the order of 0.1 sec or more for actuation.<sup>2</sup> In this time interval a hypersonic vehicle travels a distance equal to many times its length, and thus conventional methods for flight control cannot achieve rapid maneuvering.

There is little research on the effect of energy deposition for flight control. Girgis *et al.*<sup>12</sup> studied the effect of adding a continuous heated region in front of a cone cylinder at zero angle of attack at Mach 3 and showed the existence of a maximum lift to drag ratio based on the location of the heated region. Azarova *et al.*<sup>4-6</sup> examined the effect of off-axis energy discharge on the flowfield structure and aerodynamic forces on simplified aerodynamic shapes. Starikovskiy *et al.*<sup>30</sup> examined the effect of pulsed laser discharge for flight control of a small rotating projectile at Mach 3 and reported a 1° change in the projectile angle of attack with only 2 mJ of energy per pulse for a 3.9 cm long model. Kianvashrad *et al.*<sup>15</sup> evaluated an off-axis laser discharge in front of a hemisphere cylinder at Mach 2 and showed that the maximum instantaneous side force is comparable to the drag reduction. Elias *et al.*<sup>9</sup> noted that a terawatt femtosecond laser may be useful for steering a high speed vehicle.

This paper focuses on the effect of an off-axis energy discharge on the side force, drag reduction and pitching moment of a notional supersonic/hypersonic vehicle at Mach 3 and 6. A parametric study is performed to examine the effects of the energy discharge parameter  $\epsilon = E/p_\infty V$  and relative volume of the discharge to the cube radius of the body  $V/R^3$  where  $E$  and  $V$  are the energy and initial volume of the discharge and  $R$  is the radius of the body. The effect of Mach number on the forces and pitching moment is also investigated.

## 2. Description of Problem

An off-axis energy discharge is added in front of a notional supersonic/hypersonic vehicle at Mach 3 and 6. The freestream condition is air in full equilibrium at sea level conditions. Table 1 presents the freestream conditions where  $M_\infty$  is freestream Mach number,  $Re/m$  is the freestream Reynolds number per length,  $Y_{N_2}$ ,  $Y_{O_2}$ , and  $Y_{NO}$  are respectively mass fractions of  $N_2$ ,  $O_2$ , and  $NO$ ,  $T_w$  and  $T_\infty$  are respectively wall and freestream temperatures, and  $p_\infty$  is the freestream static pressure. The energy discharge is instantly added to the flow by increasing static and vibrational temperatures to the level that energy added to the heated region be equal to the discharge energy. Figure 1 shows the schematic of the off-axis energy discharge in front of the notional supersonic vehicle.

Table 1: Freestream condition

Variables	Freestream condition 1	Freestream condition 2
$M_\infty$	3	6
$Re/m$	$7 \times 10^7$	$1.4 \times 10^8$
$Y_{N_2}$	0.76	0.76
$Y_{O_2}$	0.23	0.23
$Y_{NO}$	0.01	0.01
$\frac{T_w}{T_\infty}$	1.0	1.0
$T_\infty$	288.15 K	288.15 K
$P_\infty$	101 325 Pa	101 325 Pa

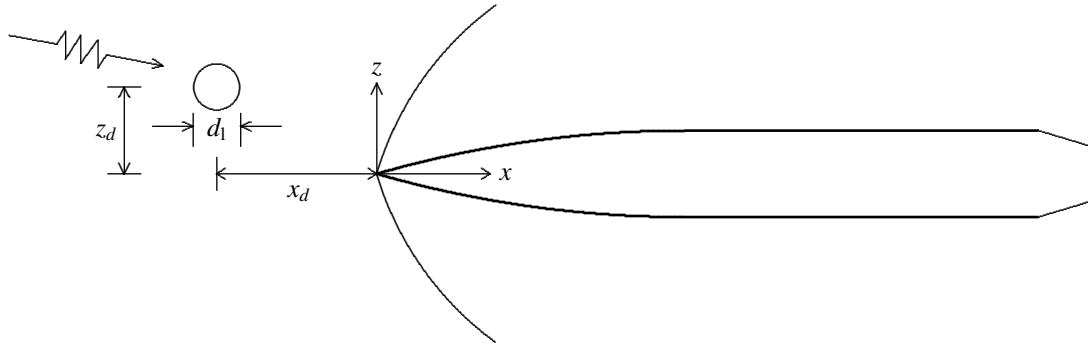


Figure 1: Schematic of an off-axis energy discharge in front of a notional vehicle

Figure 2 shows the schematic of the notional vehicle used in this paper. The body is defined by the fineness ratio  $f$ , cylindrical part radius  $R$ , cylinder length  $L_c$ , boattail length  $L_t$ , and the boattail radius  $R_t$ . The fineness ratio is defined as

$$f = \frac{L}{2R} \quad (1)$$

and the radius of the ogive is

$$R_c = 2R \left( f^2 + \frac{1}{4} \right) \quad (2)$$

Table 2 presents the geometric properties of the body used in this paper where  $L_{total} = L + L_c + L_t$ .

Table 2: Geometric properties and dimensions

$f$	$L/R$	$L_c/R$	$L_t/R$	$L_{total}/R$	$R_t/R$	$R$ (m)
3.559	7.118	8.194	1.183	16.495	0.645	0.465

To better understand the effect of the off-axis energy discharge on side force, drag reduction and pitching moment of a vehicle in supersonic and hypersonic flow, a parametric study is performed to examine the effects of the dimensionless energy discharge parameter  $\epsilon = E/p_\infty V$ , the relative size of the discharge to the body  $V/R^3$ , and freestream Mach number where  $E$  and  $V$  are the energy and initial volume of the discharge. The cases are summarized in Table 3

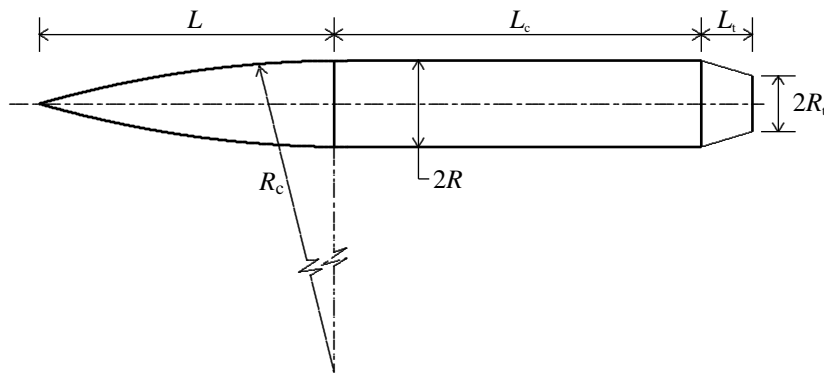


Figure 2: Schematic of a notional vehicle geometry

where the energy  $E$  corresponding to flight at sea level conditions ( $p_\infty = 101325$  Pa) is indicated. Note that the energy  $E$  is proportional to  $p_\infty$ , so that the energy required for a fixed value of  $\epsilon$  decreases with flight altitude. Cases 1 to 4 are used to study the effect of the energy added to the gas due to the energy discharge. The energy discharge size and the location of the discharge is the same for all the four cases while the amount of the energy changes.

Table 3: Energy discharge initial conditions

Case No.	$M_\infty$	$\epsilon$	$E$ (kJ) <sup>a</sup>	$\frac{T^{\text{vib}}}{T_\infty} = \frac{T}{T_\infty}$	$V/R^3$	$\frac{x_d}{R}$	$\frac{z_d}{R}$
Case 1	3	50	2.1	10.925	0.004	0.485	0.250
Case 2	3	100	4.1	19.250	0.004	0.485	0.250
Case 3	3	200	8.2	34.794	0.004	0.485	0.250
Case 4	3	400	16.3	58.549	0.004	0.485	0.250
Case 5	3	200	65.2	38.833	0.032	0.485	0.250
Case 6	6	200	8.1	35.016	0.004	0.350	0.250
Case 7	6	400	16.3	58.876	0.004	0.350	0.250

<sup>a</sup>Corresponding to flight at sea level ( $p_\infty = 101325$  Pa)

To study the effect of the energy discharge size, Cases 3 and 5 shown in Table 3 are used. In this set, the dimensionless energy deposition  $\epsilon$  and the location of the discharge is the same while the size of the discharge varies. To study the effect of Mach number, Cases 3, 4, 6, and 7 are used. In this set, the freestream Mach number is changed from 3 to 6 for two levels of  $\epsilon$  while the size and the location of the heated region are the same<sup>1</sup>. In all cases the center of the spherical discharge is located in the plane of symmetry. The energy deposition is assumed to be instantaneous, and thus the initial density of the discharge region is equal to the freestream density and the initial velocity is also equal to the freestream velocity.

The change in the forces and pitching moment is compared with the result of Missile DATCOM (v97)<sup>7</sup> for a similar geometry with two sets of fins as shown in Figure 3. The larger (forward) fins are movable while the smaller ones are assumed fixed.

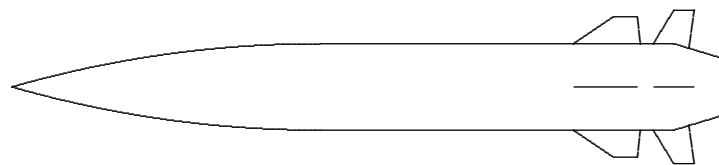


Figure 3: Schematic of a notional vehicle geometry used for Missile DATCOM (v97)

<sup>1</sup>There is a small change in the streamwise location  $x_d/R$  from Mach 3 to Mach 6.

## ENERGY DISCHARGE

### 3. Methodology

The governing equations for non-equilibrium laminar<sup>2</sup> viscous flow are described below. We consider a mixture of gases with density  $\rho_\alpha$  for  $\alpha = 1, \dots, n$  of which  $\alpha = 1, \dots, m$  constitute diatomic (or polyatomic) species and the remainder ( $i = m + 1, \dots, n$ ) represent monatomic species.

#### Conservation of Mass

The conservation of mass is

$$\frac{\partial \rho_\alpha}{\partial t} + \frac{\partial \rho_\alpha u_j}{\partial x_j} = \dot{\omega}_\alpha^{\text{spe}} + \frac{\partial}{\partial x_j} \left[ \rho D \frac{\partial Y_\alpha}{\partial x_j} \right] \quad \text{for } \alpha = 1, \dots, n \quad (3)$$

where  $\rho_\alpha$  is the density of species  $\alpha$ , the mass-averaged velocity is  $u_j$ , and  $\rho$  is the mixture density

$$\rho = \sum_{\alpha=1}^n \rho_\alpha \quad (4)$$

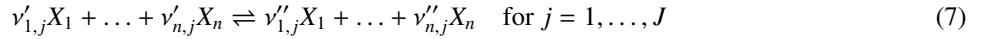
The mass fraction is defined as

$$Y_\alpha = \frac{\rho_\alpha}{\rho} \quad (5)$$

The rate of production of species  $\alpha$  is denoted as  $\dot{\omega}_\alpha^{\text{spe}}$  and defined as

$$\dot{\omega}_\alpha^{\text{spe}} = \mathcal{M}_\alpha \sum_{j=1}^J (v''_{\alpha,j} - v'_{\alpha,j}) k_{f,j} \left[ \prod_{l=1}^n \left( \frac{\rho_l}{\mathcal{M}_l} \right)^{v'_{l,j}} - \frac{1}{k_{e,j}} \prod_{l=1}^n \left( \frac{\rho_l}{\mathcal{M}_l} \right)^{v''_{l,j}} \right] \quad \text{for } \alpha = 1, \dots, n \quad (6)$$

for the general reaction expressions



where  $J$  is the number of reactions, and  $v'_{\alpha,j}$  and  $v''_{\alpha,j}$  are the stoichiometric coefficients of the reactants and products  $X_\alpha$  in the  $j^{\text{th}}$  reaction.

The diffusion of species is modeled by Fick's Law assuming a uniform diffusivity  $D$  defined by

$$D = \frac{k}{\rho c_{p_f} Le} \quad (8)$$

where  $Le = 1.0$  is the constant Lewis number,  $k$  is the mixture thermal conductivity, and  $c_{p_f}$  is the mixture specific heat at constant pressure defined by

$$c_{p_f} = \sum_{\alpha=1}^n Y_\alpha c_{p_\alpha} \quad (9)$$

#### Conservation of Momentum

The conservation of momentum is

$$\frac{\partial \rho u_i}{\partial t} + \frac{\partial \rho u_i u_j}{\partial x_j} = -\frac{\partial p}{\partial x_i} + \frac{\partial \tau_{ij}}{\partial x_j} \quad \text{for } i = 1, 2, 3 \quad (10)$$

where  $\tau_{ij}$  is the laminar viscous stress tensor defined by

$$\tau_{ij} = -\frac{2}{3} \mu \frac{\partial u_k}{\partial x_k} \delta_{ij} + \mu \left( \frac{\partial u_i}{\partial x_j} + \frac{\partial u_j}{\partial x_i} \right) \quad (11)$$

<sup>2</sup>The boundary layer on the notional vehicle is, of course, turbulent over nearly the entire vehicle length. The changes in lift, drag and moment due to the interaction of the energy deposition with the vehicle shock system are expected to be principally inviscid effects (*i.e.*, due to changes in the surface pressure on the vehicle), and thus the presence of the boundary layer is expected to be a secondary effect. Future work will include representation of the turbulent boundary layer using an eddy viscosity model.

### Conservation of Total Energy

The total energy per unit mass  $\varepsilon$  is the sum of the internal energy per unit mass  $e$  and the kinetic energy per unit mass

$$\varepsilon = e + \frac{1}{2} u_j u_j \quad (12)$$

The internal energy per unit mass  $e$  is the sum of the internal energies of each of the  $n$  species

$$e = \sum_{\alpha=1}^n \frac{\rho_{\alpha}}{\rho} e_{\alpha} \quad (13)$$

where the internal energy per unit mass of each species  $e_{\alpha}$  is the sum of an equilibrium internal energy  $e_{\alpha}^{\text{eq}}(T)$  due to random translational energy and rotational energy (in the case of molecules) at a bulk equilibrium temperature  $T$  and an internal energy  $e_{\alpha}^{\text{vib}}(T_{\alpha}^{\text{vib}})$  due to vibrational excitation (in the case of molecules)

$$e_{\alpha} = e_{\alpha}^{\text{eq}}(T) + e_{\alpha}^{\text{vib}}(T_{\alpha}^{\text{vib}}) \quad (14)$$

The equilibrium internal energy of species  $\alpha$  is

$$e_{\alpha}^{\text{eq}}(T) = h_{f_{\alpha}}^{\circ} + \int_{T_{\text{ref}}}^T c_{v_{\alpha}}(T) dT \quad (15)$$

The conservation of total energy is

$$\frac{\partial \rho \varepsilon}{\partial t} + \frac{\partial}{\partial x_j} (\rho \varepsilon + p) u_j = \frac{\partial \tau_{ij} u_i}{\partial x_j} - \frac{\partial q_j}{\partial x_j} \quad (16)$$

where the heat transfer vector is defined by

$$q_j = -k \frac{\partial T}{\partial x_j} - \sum_{\alpha=1}^m k_{\alpha}^{\text{vib}} \frac{\partial T_{\alpha}^{\text{vib}}}{\partial x_j} - \sum_{\alpha=1}^n \rho h_{\alpha} D \frac{\partial Y_{\alpha}}{\partial x_j} \quad (17)$$

The static enthalpy per unit mass for species  $\alpha$  is

$$h_{\alpha} = h_{f_{\alpha}}^{\circ} + \int_{T_{\text{ref}}}^T c_{p_{\alpha}}(T) dT \quad (18)$$

where  $h_{f_{\alpha}}^{\circ}$  is the enthalpy of formation of species  $\alpha$  at  $T_{\text{ref}}$ .

### Conservation of Vibrational Energy

The conservation of vibrational energy is

$$\frac{\partial \rho_{\alpha} e_{\alpha}^{\text{vib}}}{\partial t} + \frac{\partial \rho_{\alpha} e_{\alpha}^{\text{vib}} u_j}{\partial x_j} = - \frac{\partial q_{\alpha_j}^{\text{vib}}}{\partial x_j} + \dot{\omega}_{\alpha}^{\text{vib}} \quad \text{for } \alpha = 1, \dots, m \quad (19)$$

The heat transfer vector is

$$q_{\alpha_j}^{\text{vib}} = -k_{\alpha}^{\text{vib}} \frac{\partial T_{\alpha}^{\text{vib}}}{\partial x_j} - \rho D e_{\alpha}^{\text{vib}} \frac{\partial Y_{\alpha}}{\partial x_j} \quad (20)$$

The source term is

$$\dot{\omega}_{\alpha}^{\text{vib}} = \rho_{\alpha} \dot{e}_{\alpha}^{\text{vib}} + \dot{\omega}_{\alpha}^{\text{spe}} e_{\alpha}^{\text{vib}} \quad (21)$$

where  $\dot{e}_{\alpha}^{\text{vib}}$  is the translational-vibrational energy transfer per unit mass of species  $\alpha$ . We consider the classical Landau-Teller model<sup>32</sup>

$$\dot{e}_{\alpha}^{\text{vib}} = \frac{e_{\alpha}^{\text{vib}^*}(T) - e_{\alpha}^{\text{vib}}(T_{\alpha}^{\text{vib}})}{\tau_{\alpha}} \quad (22)$$

where  $e_{\alpha}^{\text{vib}^*}$  is the equilibrium vibrational energy per unit mass of species  $\alpha$  defined by

$$e_{\alpha}^{\text{vib}^*}(T) = \frac{R_{\alpha} \Theta_{\alpha}^{\text{vib}}}{\exp(\Theta_{\alpha}^{\text{vib}}/T) - 1} \quad (23)$$

## ENERGY DISCHARGE

and  $\tau_\alpha$  is the relaxation time<sup>25</sup> of species  $\alpha$  defined by

$$\tau_\alpha = \frac{\sum_{\beta=1}^n M_\beta}{\sum_{\beta=1}^n M_\beta \tau_{\alpha\beta}^{-1}} \quad (24)$$

where  $M_\alpha = \rho_\alpha / \mathcal{M}_\alpha$  is the molar concentration of species  $\alpha$  and  $\tau_{\alpha\beta}$  is the characteristic relaxation time of species  $\alpha$  resulting from collisions with species  $\beta$  defined by<sup>25</sup>

$$\tau_{\alpha\beta} = \frac{1}{p} \exp \left[ A_{\alpha\beta} \left( T^{-\frac{1}{3}} - B_{\alpha\beta} \right) - 18.42 \right] \quad (25)$$

where  $\tau_{\alpha\beta}$  is in seconds and  $p$  is in atmospheres, and

$$A_{\alpha\beta} = 0.00116 \mathcal{M}_{\alpha\beta}^{\frac{1}{2}} \Theta_\alpha^{\text{vib} \frac{4}{3}} \quad \text{and} \quad B_{\alpha\beta} = 0.015 \mathcal{M}_{\alpha\beta}^{\frac{1}{4}} \quad (26)$$

and the averaged molecular weight is defined by

$$\mathcal{M}_{\alpha\beta} = \frac{\mathcal{M}_\alpha \mathcal{M}_\beta}{\mathcal{M}_\alpha + \mathcal{M}_\beta} \quad (27)$$

where  $\mathcal{M}_\alpha$  is the molecular weight of species  $\alpha$ . Note that the second term in the numerator in Eq. (20) is multiplied by  $\rho_\alpha$  in Eq. (19) and is thus  $\rho_\alpha e_\alpha^{\text{vib}}$ . In the second term in Eq. (19), there are two possible choices for  $e_\alpha^{\text{vib}}$  namely,  $e_\alpha^{\text{vib}} = \frac{R_\alpha \Theta_\alpha^{\text{vib}}}{\exp(\Theta_\alpha^{\text{vib}}/T) - 1}$  and  $e_\alpha^{\text{vib}} = \frac{R_\alpha \Theta_\alpha^{\text{vib}}}{\exp(\Theta_\alpha^{\text{vib}}/T_\alpha^{\text{vib}}) - 1}$ .

### Equation of State

The equation of state is

$$p = T \sum_{\alpha=1}^n \rho_\alpha R_\alpha \quad (28)$$

where the gas constant  $R_\alpha$  for species  $\alpha$  is

$$R_\alpha = \frac{\mathcal{R}}{\mathcal{M}_\alpha} \quad (29)$$

where  $\mathcal{R}$  is the Universal Gas Constant.

### Thermodynamic Data and Transport Properties

The species thermodynamic data and species transport properties are obtained from the Gupta, Yos, Thompson, and Lee<sup>13</sup> (NASA-RP-1232) database. The mixture viscosity  $\mu$  and thermal conductivity  $k$  are determined by Wilke's Rule.<sup>33</sup> The vibrational thermal conductivity of species  $\alpha$  is

$$k_\alpha^{\text{vib}} = \mu_\alpha R_\alpha \quad (30)$$

where  $\mu_\alpha$  and  $R_\alpha$  are the molecular viscosity and gas constant for species  $\alpha$ , respectively.

### Boundary Conditions

The computational domain is shown in Fig. 4. Since the problem has a plane of symmetry, only half of the domain has been modeled. The computational domain consists of 19.6 M cells with the grid properties shown in Table 4. The boundary conditions of the computational domain are defined using colored surfaces. The red surfaces are fixed boundary condition at the freestream values. The green surface is the outflow zero-gradient boundary condition. The blue surface is the symmetry plane with the symmetry boundary condition. The black surface of the notional vehicle is non-catalytic ( $\partial Y_\alpha / \partial n = 0$  where  $n$  is the normal distance to the boundary) no-slip isothermal wall.

To solve the problem, first the flowfield is converged to steady state before adding any discharge. Then a spherical region of diameter  $d_l$  with higher static and vibrational temperatures is added to the converged flowfield which is the heated region due to the energy discharge.

### Numerical Algorithm

A block structured finite volume C++ code developed by the authors solves the governing equations. The code is parallelized using Message Passing Interface (MPI). The Roe's method<sup>28</sup> with the second-order Monotone Upstream Scheme for Conservation Laws<sup>18</sup> (MUSCL) reconstruction are used to discretize the inviscid fluxes. A second-order central differencing method discretizes the viscous fluxes. The Data Parallel Line Relaxation (DPLR) time integration of Wright *et al*<sup>35</sup> is incorporated to achieve high computational efficiency.

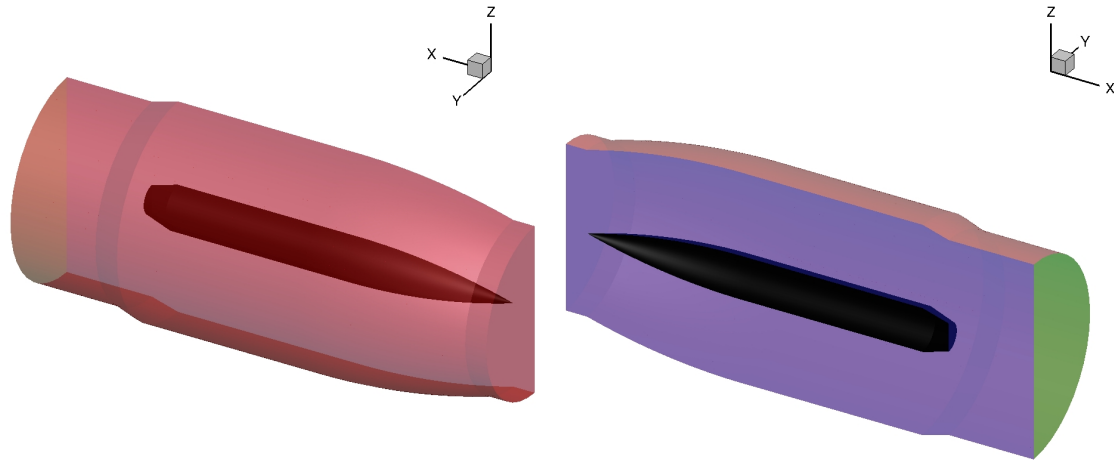


Figure 4: Computational domain

Table 4: Grid properties

$\Delta\xi$ (mm)	$\Delta\eta_{min}$ (mm)	$\Delta\zeta$ (degree)
2.26	1.86	9

NOTE:

 $\Delta\xi$  is spacing along the wall $\Delta\eta$  is spacing normal to the wall $\Delta\zeta$  is the axial spacing

## 4. Results

In this section, the effect of the energy added to the flow, the size of the heated region, and Mach number on the side force, drag reduction, and pitching moment are examined. Table 3 presents the cases used for studying these effects. The drag, side force, and pitching moment coefficients are defined as<sup>3</sup>

$$C_D = \frac{F_x}{\frac{1}{2}\rho_\infty U_\infty^2 \pi R^2} \quad (31)$$

$$C_Z = \frac{F_z}{\frac{1}{2}\rho_\infty U_\infty^2 \pi R^2} \quad (32)$$

$$C_m = \frac{M_y}{\frac{1}{2}\rho_\infty U_\infty^2 \pi R^2 L_{total}} \quad (33)$$

where  $F_x$  and  $F_z$  are respectively drag and side forces,  $M_y$  is the pitching moment,  $\rho_\infty$  is the freestream density, and  $U_\infty$  is the freestream velocity. Forces and pitching moment are calculated over the entire surface of the body (not on the half of the body is used in the simulations). The pitching moment is calculated about the middle of the body. The dimensionless time is defined as

$$\tau = \frac{tU_\infty}{R} \quad (34)$$

where  $t$  is dimensional time.

### 4.1 Effect of Energy Level

To study the effect of the energy added to the gas on the produced side force, drag reduction, and pitching moment, the dimensionless energy parameter  $\epsilon = E/\rho_\infty V$  is varied while the location and size of the energy deposition remains constant. Cases 1 to 4 of Table 3 are the four cases used for this study. Figure 5 shows the variation of drag reduction,

<sup>3</sup>Note that the definition for  $C_m$  is identical to its definition in Missile DATCOM (v97). See p. 59 in Blake.<sup>7</sup>

## ENERGY DISCHARGE

side force and pitching moment coefficient versus time for all four cases. The interaction of the blast wave of the heated region and the shock created by the body creates a transmitted shock. This transmitted shock interacts with the body and increases the surface pressure and therefore increases the drag force to a maximum value while creating a negative side force. The interaction of the heated region with the shock forms an expansion wave which reduces the pressure on the body and thus reduces the drag while increasing the side force to a maximum with a positive sign. A vortex forms as a result of the Richtmyer-Meshkov instability of the interaction of heated region and the shock. This vortex moves along the body and changes the drag force while its effect on the side force is negligible especially for the lower energy levels. The interaction of this vortex with the expansion wave at the tail of the body and the wake of the body produces a sudden drag reduction. At the same time, a peak in the side force forms in the negative direction. It can be seen from Figure 5 that increasing the dimensionless energy of the heated region makes stronger interactions and thus causes a higher peaks and troughs in the force and pitching moment coefficients.

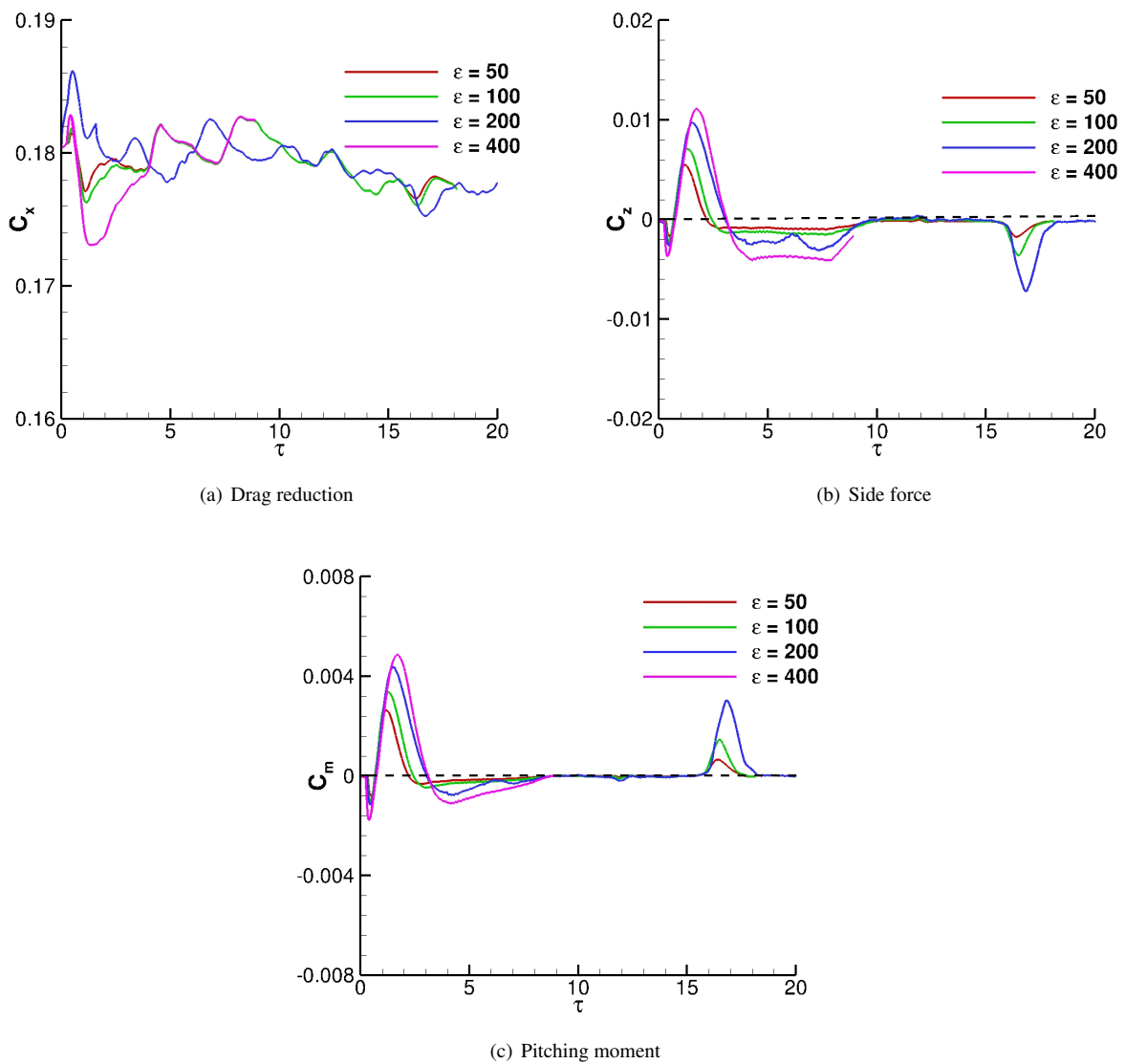


Figure 5: Effect of dimensionless energy on drag reduction, side force, and pitching moment for  $M_\infty = 3$  and  $V/R^3 = 0.004$

The maximum pitching moment due to the interaction of the energy discharge with the vehicle varies from 0.0024 to 0.0048 for  $\epsilon = 50$  to 400. Note that the peak value does not scale linearly with  $\epsilon$ . An eightfold increase in  $\epsilon$  results in a doubling of the maximum pitching moment, and the change in peak value from  $\epsilon = 200$  to 400 is negligible. The interaction dimensionless time interval corresponding to the changes in  $C_m$  is  $\Delta\tau \approx 5$  which corresponds to the vehicle traveling a distance of approximately 0.3 times its length ( $\Delta t U_\infty / L_{total} = 0.3$ ).

The pitching moment coefficient of the vehicle shown in Figure 3 is calculated using Missile DATCOM (v97) at Mach 3. The dimensions of the body are the same for the simulations and the Missile DATCOM results. The magnitude of the pitching moment about the midpoint of the vehicle resulting from a  $20^\circ$  deflection of the first finset at zero angle of attack is 0.075 and the corresponding dimensionless time for a 0.1 s actuation is  $\Delta\tau = 220$  ( $\Delta t U_\infty / L_{total} = 13.3$ ). Thus, the energy deposition achieves a peak pitching moment of 3.2% to 6.4% of the deflected fins pitching moment; however, the effect is 44 times faster. Consequently, multiple energy pulses may have the potential to achieve substantial change in the vehicle direction.

#### 4.2 Effect of the Heated Region Size

To study the effect of the size of the heated region relative to the body  $V/R^3$  on the side force, drag reduction and pitching moment, two different values of  $V/R^3$  are considered as indicated in Table 3 by Cases 3 and 5, while the dimensionless energy  $\epsilon$  and location of the heated regions are the same. Figure 6 shows the variation of drag reduction, side force and pitching moment coefficient versus time for the three cases. From Figure 6, it can be seen that the larger size of the heated region relative to the body produces a higher side force and pitching moment coefficients in both positive and negative direction. However, the increase in the maximum pitching moment does not scale linearly with  $V/R^3$ . An increase in  $V/R^3$  by a factor of 800% results in an increase in the peak pitching moment coefficient of 60%. The drag reduction increases dramatically by increasing the size.

#### 4.3 Effect of Mach Number

To study the effect of Mach number on the drag reduction, side force and pitching moment, Cases 3, 4, 6 and 7 of Table 3 are used. In Cases 3 and 4, the Mach number is 3 while for Cases 7 and 8 the Mach number is 6. Two levels of dimensionless energy deposition ( $\epsilon = 200$  and 400) are considered while the vertical location of the discharge ( $z_d/R$ ) is constant and there is a little change in horizontal distance from the vehicle tip ( $x_d/R$ ). Figure 6 shows the change in drag, side force and pitching moment coefficients versus time. From this figure, it is visible that the drag force coefficients are smaller at Mach 6 in comparison with Mach 3 while they have relatively the same side force coefficient. Therefore, the resultant pitching moment about the mid-length of the vehicle is also small for Mach 6. Missile DATCOM (v97) calculates a pitching moment coefficient of 0.043 for a  $20^\circ$  deflection of the first finset at zero angle of attack. The corresponding dimensionless time for a 0.1 s actuation is  $\Delta\tau = 440$  ( $\Delta t U_\infty / L_{total} = 26.6$ ). The energy deposition at Mach 6 achieves a peak pitching moment of 3.7% of the deflected fins pitching moment; however, the effect is 88 times faster. Consequently, multiple energy pulses may have the potential to achieve substantial change in the vehicle direction.

### 5. Conclusion

The effect of off-axis energy discharge in front of a notional supersonic/hypersonic vehicle at Mach 3 and 6 is examined. The off-axis energy discharge changes the force distribution over the body and thus creates a side force and changes the drag force. As a result, there is a change in the pitching moment acting on the body. The effect of the dimensionless energy deposition  $\epsilon$ , the relative size of the heated region  $V/R^3$  and the freestream Mach number  $M_\infty$  on the forces and pitching moment are examined. The peak pitching moment coefficient increases with increasing  $\epsilon$  at fixed  $V/R^3$ ; however, the increase is not linear in  $\epsilon$  and a saturation effect eventually occurs whereby increasing  $\epsilon$  does not result in a significant change in the peak pitching moment coefficient. The peak pitching moment increases with  $V/R^3$  for fixed  $\epsilon$ ; however, the increase is sublinear. The peak pitching moment coefficient decreases with Mach number for fixed  $\epsilon$  and  $V/R^3$ . Energy deposition achieves a peak pitching moment coefficient from 3.2% to 6.4% of the value predicted by Missile DATCOM (v97) for the same vehicle with a  $20^\circ$  finset deflection. However, the duration of the pitching moment change is 44 to 88 times faster than the actuation time for the finset deflection, thus indicating the possibility of energy deposition for flight control.

## ENERGY DISCHARGE

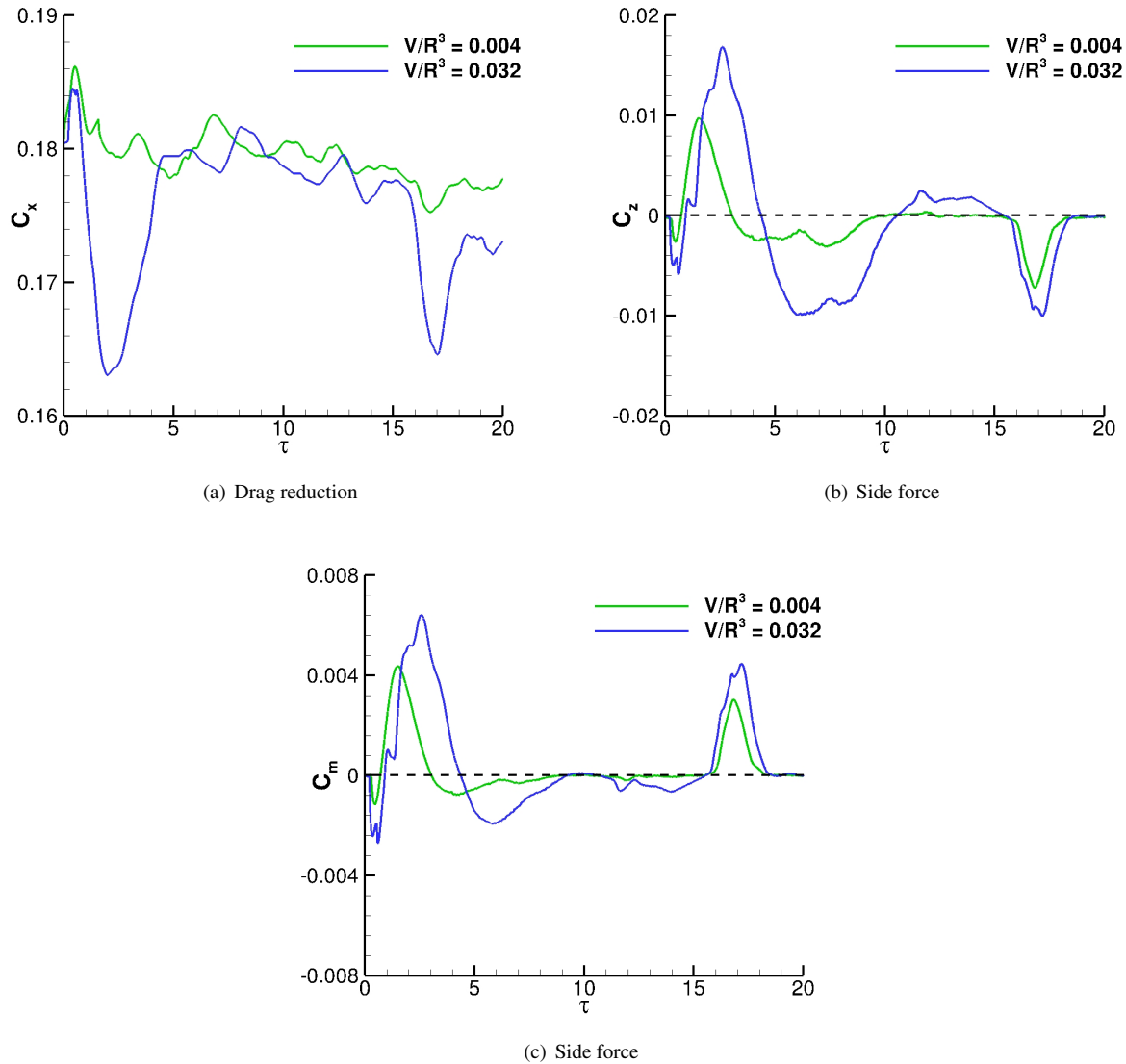


Figure 6: Effect of the size of heated region on drag reduction, side force, and pitching moment for  $M_\infty = 3$  and  $\epsilon = 200$

## 6. Acknowledgments

Computer resources for this research were provided by the Rutgers Discovery Informatics Institute RDI<sup>2</sup> supported by Rutgers and the State of New Jersey.<sup>26</sup>

## References

- [1] R Adelgren, H Yan, G Elliott, D Knight, T Beutner, and A Zheltovodov. Control of Edney IV Interaction by Pulsed Laser Energy Deposition. *AIAA Journal*, 43(2):256–269, 2005.
- [2] K Anderson and D Knight. Plasma Jet for Flight Control. *AIAA Journal*, 50(9):1855–1872, 2012.
- [3] V Artem'ev, V Bergel'son, I Nemchinov, T Orlova, A Smirnov, and V Khazins. Change of Regime in Supersonic Flow Past on Obstacle Preceded by a Thin Channel of Reduced Density. *Izvestiya Akademii Nauk SSSR, Mekhanika Zhidkosti Gaza*, 5:146–151, September-October 1989.

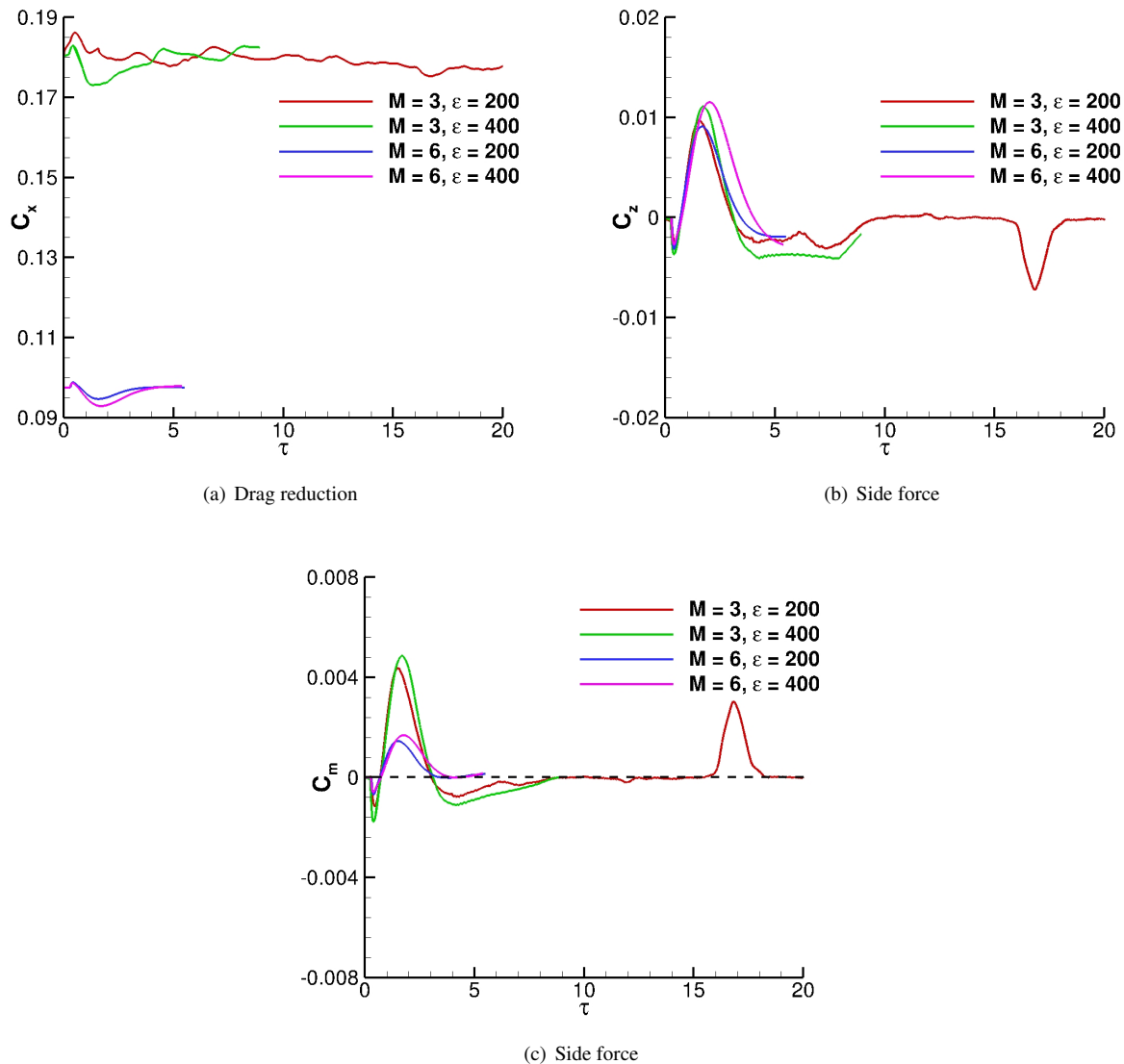


Figure 7: Effect of Mach number on drag reduction, side force, and pitching moment for  $\epsilon = 200$  and  $400$  and  $V/R^3 = 0.004$

- [4] O Azarova. Simulation of Stochastic Pulsating Flows with Instabilities Using Minimum-Stencil Difference Schemes. *Computational Mathematics and Mathematical Physics*, 49(8):1397–1414, August 2009.
- [5] O Azarova, D Knight, and Y Kolesnichenko. Flowfields around Supersonic Aerodynamic Bodies under the Action of Asymmetric Energy Release. In P Reijasse, D Knight, M. Ivanov, and I. Lipatov, editors, *Progress in Flight Physics*, volume 5 of *EUCASS Book Series, Advances in Aerospace Sciences*, pages 139–152. European Conference for Aerospace Sciences, Torus Press.
- [6] O Azarova, D Knight, and Y Kolesnichenko. Flow Control via Instabilities, Vortices and Steady Structures under the Action of External Microwave Energy Release. *Proceedings of the Institution of Mechanical Engineers, Part G: Journal of Aerospace Engineering*, 227(9):1498–1515, August 2013.
- [7] W Blake. MISSILE DATCOM - User Manual - 1997 FORTRAN 90 Revision. Technical Report AFRL-VA-WP-TR-1998-3009, Air Force Research Laboratory, February 1998.
- [8] S Desai, V Kulkarni, H Gadgil, and B John. Aerothermodynamic Considerations for Energy Deposition Based Drag Reduction Technique. *Applied Thermal Engineering*, 122:451–460, July 2017.

## ENERGY DISCHARGE

- [9] P Elias, N Severac, J Luysen, Y André, I Doudet, B Wattellier, J Tobeli, S Albert, B Mahieu, R Bur, A Mysyrowicz, and A Houard. Improving Supersonic Flights with Femtosecond Laser Filamentation. *Science Advances*, 4(11):1–5, November 2018.
- [10] E Erdem, K Kontis, and L Yang. Steady Energy Deposition at Mach 5 for Drag Reduction. *Shock Waves*, 23(4):285–298, July 2013.
- [11] V Fomin, P Tretyakov, and J Taran. Flow Control Using Various Plasma and Aerodynamic Approaches (Short Review). *Aerospace Science and Technology*, 8(5):411–421, July 2004.
- [12] I Girgis, M Shneider, S Macheret, G Brown, and R Miles. Steering Moments Creation in Supersonic Flow by Off-Axis Plasma Heat Addition. *Journal of Spacecraft and Rockets*, 43(3):607–613, May-June 2006.
- [13] R Gupta, J Yos, R Thompson, and K Lee. A Review of Reaction Rates and Thermodynamic and Transport Properties for an 11-Species Air Model for Chemical and Thermal Nonequilibrium Calculations to 30000 K. Reference Report 1232, NASA, 1990.
- [14] N Kianvashrad and D Knight. Non-Equilibrium Effects of Interaction of Laser Discharge with Hemisphere-Cylinder in Supersonic Flow. AIAA Paper 2018-3757, American Institute of Aeronautics and Astronautics, June 2018.
- [15] N Kianvashrad, D Knight, S Wilkinson, A Chou, G Beeler, and M Jangda. Effect of Off-Body Laser Discharge on Drag Reduction of Hemisphere Cylinder in Supersonic Flow-Part II. AIAA Paper 2018-1433, American Institute of Aeronautics and Astronautics, January 2018.
- [16] N Kianvashrad, D Knight, S Wilkinson, A Chou, R Horne, G Herring, G Beeler, and M Jangda. Effect of Off-Body Laser Discharge on Drag Reduction of Hemisphere Cylinder in Supersonic Flow. AIAA Paper 2017-3478, American Institute of Aeronautics and Astronautics, June 2017.
- [17] J Kim, A Matsuda, T Sakai, and A Sasoh. Wave Drag Reduction with Acting Spike Induced by Laser-Pulse Energy Depositions. *AIAA Journal*, 49(9):2076–2078, 2011.
- [18] D Knight. *Elements of Numerical Methods for Compressible Flows*. Cambridge University Press, New York, 2006.
- [19] D Knight. Survey of Aerodynamic Drag Reduction at High Speed by Energy Deposition. *Journal of Propulsion and Power*, 24(6):1153–1167, November-December 2008.
- [20] D Knight. *Energy Deposition for High-Speed Flow Control*. Cambridge University Press, New York, 2019.
- [21] D Knight, Y Kolesnichenko, V Brovkin, D Khmara, V Lashkov, and I Mashek. Interaction of Microwave-Generated Plasma with a Hemisphere Cylinder at Mach 2.1. *AIAA Journal*, 47(12):2996–3010, 2009.
- [22] K Kremeyer, K Sebastian, and C Shu. Computational Study of Shock Mitigation and Drag Reduction by Pulsed Energy Lines. *AIAA Journal*, 44(8):1720–1731, 2006.
- [23] S Kuo. Plasma Mitigation of Shock Wave: Experiments and Theory. *Shock Waves*, 17(4):225–239, December 2007.
- [24] V Lashkov, I Mashek, Y Anisimov, V Ivanov, Y Kolesnichenko, M Ryvkin, and A Gorynya. Gas Dynamic Effect of Microwave Discharge on Supersonic Cone-shaped Bodies. AIAA Paper 2004-0671, American Institute of Aeronautics and Astronautics, January 2004.
- [25] R Millikan and D White. Systematics of Vibrational Relaxation. *The Journal of Chemical Physics*, 39(12):3209–3213, 1963.
- [26] M Parashar, M Brennan-Tonetta, I Rodero, and J Villalobos. High Performance Computing at the Rutgers Discovery Informatics Institute. Technical report, November 2018.
- [27] D Riggins, H Nelson, and E Johnson. Blunt-Body Wave Drag Reduction Using Focused Energy Deposition. *AIAA Journal*, 37(4):460–467, 1999.
- [28] P Roe. Approximate Reimann Solvers, Parameter Vectors, and Difference Schemes. *Journal of Computational Physics*, 43(2):357–372, October 1981.

- [29] E Schülein, A Zheltovodov, E Pimonov, and M Loginov. Experimental and Numerical Modeling of the Bow Shock Interaction with Pulse-Heated Air Bubbles. *International Journal of Aerospace Innovations*, 2(3):165–188, 2010.
- [30] A Starikovskiy, C Limbach, and R Miles. Trajectory Control of Small Rotating Projectiles by Laser Discharges. AIAA Paper 2016-4308, American Institute of Aeronautics and Astronautics, June 2016.
- [31] P Tretyakov, A Garanin, V Kraynev, A Tupikin, and V Yakovlev. Investigation of Local Laser Energy Release Influence on Supersonic Flow by Methods of Aerophysical Experiments. In *International Conference on Methods of Aerophysical Research, Novosibirsk, Russia*, 1996.
- [32] W Vincenti and C Kruger. *Introduction to Physical Gas Dynamics*. Krieger Publishing Company, Malabar, Florida, 1965.
- [33] C. Wilke. A Viscosity Equation for Gas Mixtures. *Journal of Chemical Physics*, 18(4):517–519, 1950.
- [34] J Wilkerson, D Van Wie, and B Cybyk. Numerical Assessment of Heterogeneous Plasma Discharge Effects on Supersonic Forebody Drag. AIAA Paper 2003-526, American Institute of Aeronautics and Astronautics, January 2003.
- [35] M Wright, D Bose, and G Candler. A Data-Parallel Line Relaxation Model for the Navier-Stokes Equations. *AIAA Journal*, 36(9):1603–1609, 1998.